Image Analysis of Bubbling Mode Condensation Oscillations in Horizontal Sparger

Hujala Elina, Tanskanen Vesa, Patel Giteshkumar, Hyvärinen Juhani

IMAGE ANALYSIS OF BUBBLING MODE CONDENSATION OSCILLATIONS IN HORIZONTAL SPARGER

Elina Hujala, Vesa Tanskanen, Giteshkumar Patel and Juhani Hyvärinen
Nuclear Engineering, LUT School of Energy Systems, Lappeenranta-Lahti University of Technology LUT, Yliopistonkatu 34, 53850 Lappeenranta, Finland
Elina.Hujala@lut.fi, Vesa.Tanskanen@lut.fi, Giteshkumar.Patel@lut.fi, Juhani.Hyvarinen@lut.fi

ABSTRACT

Pattern recognition based image analysis algorithm was developed for analyzation of bubbling mode condensation oscillations in horizontal spargers. Safety relief valve test rig SEF-POOL was filled with a heated up (85 °C) water. The high mass flux steam (180 kg/(m^{2}s) was pushed through a horizontal sparger (16 mm). The SEF-INF2 experiment was recorded using a high-speed video camera with a frame rate of 2800 fps. An improved image processing and analysis procedure have been applied to the video material. A new algorithm can deal with multiple simultaneous bubbles that can disappear for a while during the condensation. Features of the oscillating bubbles, e.g. formation frequency, lifetime, surface velocity, and acceleration, have been evaluated. The evaluated properties of the bubbles were also applied to CFD simulations, where the algorithm was used to determine critical wavelengths in succession to establish the most suitable grid density for the simulations. The preliminary results look promising. A large frame rate (2800 fps) yields significant information about condensation oscillations. Consequently, the bubble properties and oscillations are captured better than before. The accuracy of the pattern recognition algorithm has also been increased. 67 bubbles were tracked. Bubble mean lifetime was 0.0247 s, mean time difference between bubble formations was 0.0140 s which corresponds to 71.6 Hz formation frequency. 2D surface velocities and accelerations can now be estimated in all angles, which makes image analysis an effective tool in validation efforts of interfacial area and heat transfer models for numerical.

KEYWORDS
two-phase flow, image analysis, condensation oscillation, sparger

1. INTRODUCTION

All operating boiling water reactors (BWRs) use pressure suppression containment [1]. Usually, two kinds of steam injection mechanisms are used: the safety/relief valve (SRV) spargers and the blowdown pipes. The use of these mechanisms during normal operation or in a possible loss-of-coolant accident (LOCA) may cause structural loads to the suppression pool due to the rapid condensation of the steam. Experimental research and computational fluid dynamics (CFD) simulations have widely been used to study these structural loads. As the CFD modeling of two-phase flow has its challenges [2], new measuring techniques for CFD model validation purposes have been put into operation, such as particle image velocimetry (PIV), wire-mesh sensors (WMS), and high-speed cameras. Different camera types, from movie cameras to modern high-speed cameras, have been used to record experiments for decades, but not until lately, the high-speed cameras are used to record the experiments in more through manner [3-5]. As the amount of experimental data has increased significantly, the use of high-speed cameras permits more feasible data analysis.

Previously, a pattern recognition methods based algorithm was applied for vertical vent pipe experimental data [5-7], where the algorithm was used to recognize large steam bubbles from the video material and

evaluate the basic properties of the bubbles. The image analysis data of the vertical vent pipe algorithm provided also initial parameters and boundary conditions for CFD simulations. When the algorithm was successfully applied to vertical cases, a decision was made to expand the algorithm to cover horizontal spargers.

A separate effect test facility (SEF-POOL) of LUT University makes it possible to study the momentum caused by the oscillating condensing steam jets injected into the water pool using sparger orifice. A phenomenological reference system for the SEF-POOL facility is the SRV sparger pipe of a BWR. The compact size scale of the SEF-POOL facility provides good conditions for high-speed video recording and for other measuring techniques as well. The initial results from the SEF-POOL experiments have currently been analyzed for the validation purposes of the effective heat/momentum source (EHS/EMS) models [8, 9] in KTH, and 3D CFD simulations of the tests have been done by VTT [10].

The idea of the SEF-INF test series of SEF-POOL was to produce validation data for large interface two-fluid condensation and interfacial area density CFD models in sparger cases. Due to the origins of such models, the best initial validation case for them would be a test containing visible large continuous interface, i.e. a large condensing bubble. However, such conditions provide also a good environment for extending the pattern recognition algorithm for large bubbles by Hujala et. al. [5] to be applicable in sparger studies, which, in turn, could be used in CFD model validation purposes as well.

This paper presents the improvements made to the developed pattern recognition based image analysis algorithm for horizontal sparger cases, and the preliminary results of the image analysis of bubbling mode condensation oscillations recorded during the SEF-INF2 experiment of the SEF-POOL test facility

2. SEF-POOL TEST FACILITY AND SEF-INF2 EXPERIMENT

The SEF-POOL test facility was designed for the direct measurement of the effective momentum induced by a steam injection through a single hole or a few sparger holes. Fig. 1 shows a general view of the SEF-POOL test facility.

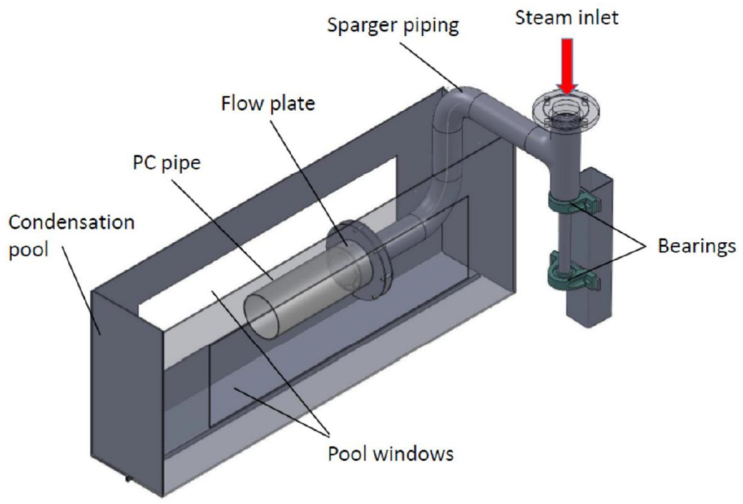

Figure 1. General view of the SEF-POOL test facility

The facility consists of an open, water-filled, uninsulated, 1500 mm long, 300 mm wide, and 600 mm high stainless steel condensation pool and an insulated stainless steel DN80 line ending up to an orifice plate. Steam line, connected to a steam generator, runs downwards from the top of the condensation pool and bends to the horizontal direction. The steam is injected through the orifice plate, which has a one or multiple orifices. Steam condensates inside an open polycarbonate (PC) pipe connected to the flow plate system, which guides replacement water to the PC tube. Different diameters of orifices can be used and the PC pipe is removable if not needed in the experiment. Large windows along both sides of the pool enable the use of high-speed video cameras and different lighting conditions. Amore detailed description of the SEF-POOL test facility is presented in [11].

2.1 SEF-INF2 Experiment

A short test series, named SEF-INF, of the SEF-POOL facility, was carried out to reach the condensation oscillation (CO) and bubbling condensation oscillation modes (BCO) obtaining good quality high-speed video samples of condensing jets and bubbles. SEF-INF series consists of two experiments, SEF-INF1 and SEF-INF2, which had a different steam mass flow rates, 65 g/s, and 36 g/s, respectively. The SEF-INF2 test was chosen for this study. The initial water level on the pool was 0.47 m, and the initial water temperature was 12 ºC. A flow plate with a single, diameter of 16 mm orifice, was used. The steam mass flow rate was kept constant (~36 g/s), when the corresponding steam mass flux was approximately 180 kg/(m^{2}s). During the test, the temperature of the condensation pool water T_w increased up to 85 ºC. Six video shots, named as SEF-INF2-1…SEF-INF2-6, in different pool water temperatures (44 ºC - 85 ºC) were recorded. The frame rate of 2800 fps was used in the video recordings, while the length of each video shot was approximately 1 s limited by the cameras data storage capacity. Fig. 2 shows the image sequence of each video shot.

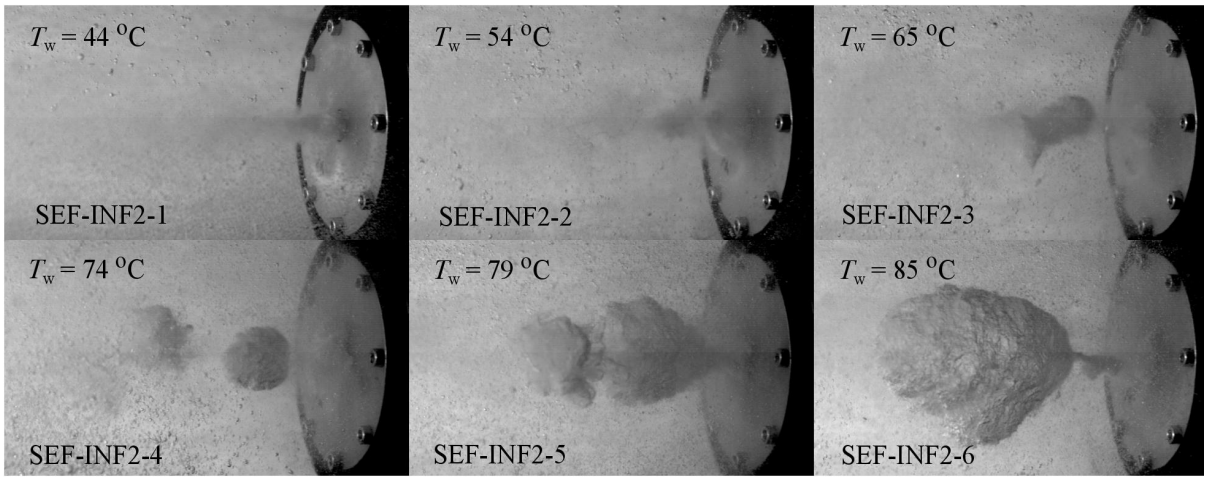

Figure 2. Examples of SEF-INF2-1…SEF-INF2-6 video frames.

A condensation mode of each test was determined using a regime map of Song et. al. [12], presented in Fig. 3. The regime map in Fig. 3 and images from the tests SEF-INF2-1…SEF-INF2-6 in Fig. 2 showed that the medium temperature (44 ºC-65 ºC) samples SEF-INF2-1…SEF-INF2-3 are within CO mode. The warm temperature tests SEF-INF2-4 and SEF-INF2-5 are approaching the BCO mode, and the hot temperature test SEF-INF2-6 seems to be clearly within the BCO mode.

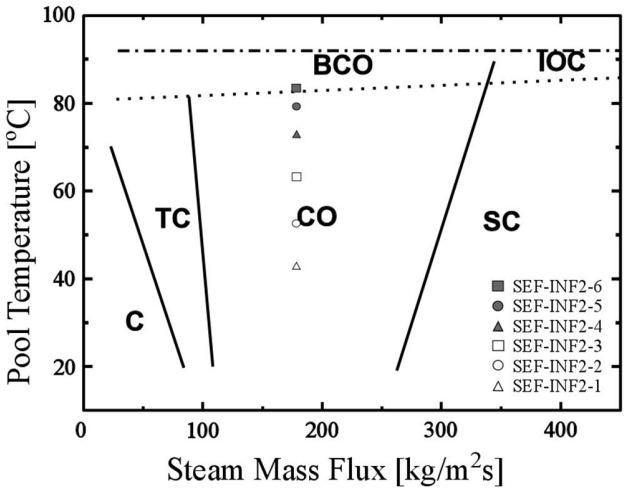

Figure 3. Regime map of Song et al., [12], in which, C refers chugging, TC transitional chugging, CO condensation oscillation, BCO bubbling condensation oscillation, SC stable condensation, and IOC interfacial oscillation condensation mode.

The regime map of Song et. al. corresponds well to the visual observations of SEF-INF2 video samples. The bubbles in SEF-INF2-6 have a clear continuous interface (called a large interface in CFD simulations) and they detach from the orifice and condense in a frequent manner. Thus, a sample of BCO mode is interesting for both, the numerical large interface condensation modeling and the image analysis of large bubbles. Furthermore, these warmed up pool BCO conditions are less frequently measured amongst and modeled modes. Thus, the SEF-INF2-6 test was chosen as a reference test for this study.

3. ANALYSIS METHODS AND LIMITATIONS

In the previously analyzed large vent blowdown experiments [5-7], steam was pushed through a large diameter (DN100/DN200) vertical blowdown pipe to the pressurized suppression pool. Typically, the system created a single steam bubble, which built up slowly, returned inside the pipe or condensed rapidly to the pool water due to chugging. The bubbles hardly ever detached from the outlet of the pipe, and usually, only one bubble appeared at a time. The pattern recognition and data analysis algorithm were successfully applied to the vertical blowdown pipe experiments, and estimations of basic features of the bubbles such as volume, surface area, vertical formation and break up velocity and acceleration of the bubble surface were obtained [5].

Because the use of image analysis and pattern recognition methods for the analysis of transient two-phase flow experiments has great potential, the image analysis algorithm has been improved further to encompass the properties of multiple simultaneous bubbles and arbitrary angles of the bubble surface velocity and acceleration.

In a horizontal sparger operating within BCO mode, the steam pushes through the orifice; bubble grows up, detaches from the orifice plate, then oscillates for a while and finally condensates disappearing. A new bubble might grow up immediately after the detachment of the previous bubble, or after a while. Probably due to the pressure oscillations, some of the bubbles or swarm of its residue bubbles even grow back before finally condensing.

When analyzing this kind of experiment with reasonable effort, a suitable image analysis algorithm is needed. The extended algorithm consists of three parts: pre-processing part, where all image processing is performed, simplified pattern recognition part, where the edges of the steam bubbles have been detected, and a post-processing part, where all image analysis and data collection takes place.

In the SEF-INF2 video material, the frames are clipped in such a way that the whole path of a bubble fits in the image. In other words, when the bubble leaves the image it is due to condensation, not just passing the border of the image. In the SEF-INF2 material, the same frame contains usually two to three bubbles – one nascent bubble, one oscillating bubble, and one vanishing bubble. Due to this more complex bubble cycle compared to the vertical blowdowns, some new analysis techniques have been applied.

The image analysis was made using MATLAB packages [13]. Pre-processing and recognition of bubble boundaries are based on the pattern recognition algorithm for the vertical blowdown pipe experiments, [5], where every pixel of the grayscale image has a certain color limit threshold. In order to distinguish a bubble, the image is compared to an empty background image, and the output image should contain only the changed pixel values that are recognized as bubble parts. The method is easy in theory, but has its weaknesses in changing conditions, for example in differing lighting levels, the appearance of a swarm of small bubbles, and bubbles due to the presence of incondensable gases. Fig. 4 shows examples of bubble borders using edge detection.

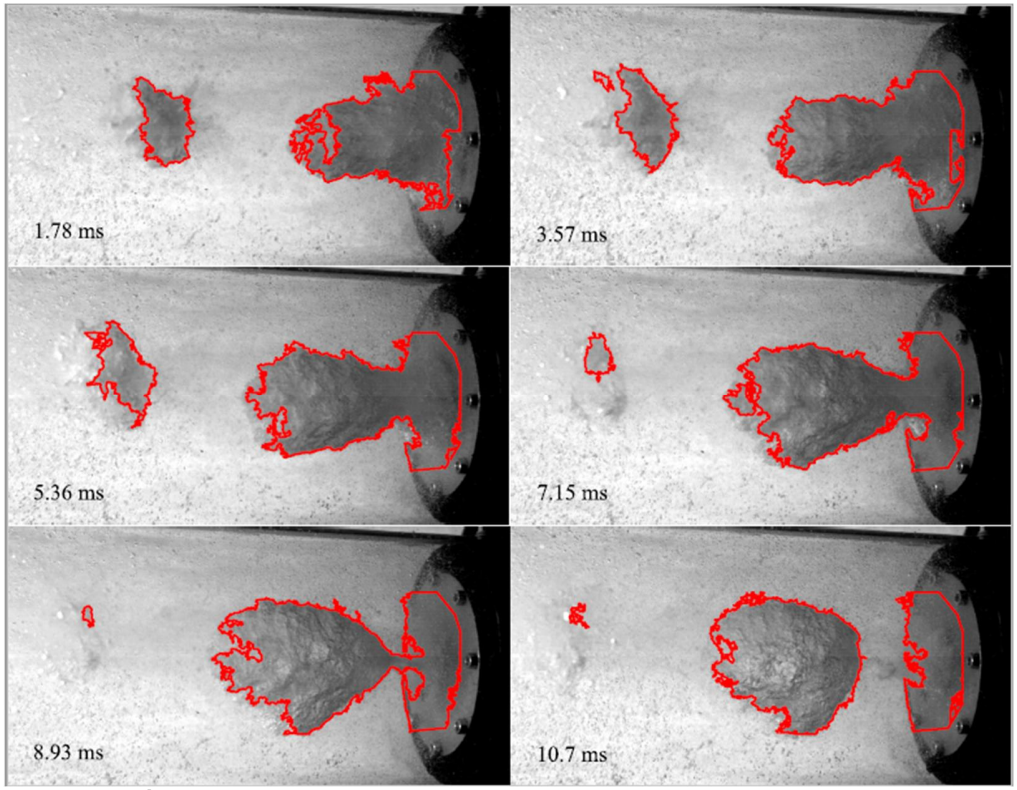

Figure 4. Every 5th frame of a 9 ms video sample from a SEF-INF2 test. Recognized boundaries are marked as red.

As is visible in Fig. 4, edge detection of the bubble boundaries has some issues due to brightness changes of the bubble surface. In these areas, the threshold limit cannot be found properly and the threshold value

of the bubble is too near to the threshold value of the background. In vertical vent cases, the threshold difference between the bubbles and the background was clear. Thus, improvements were needed with the SEF-INF2 case.

When the shadows of the bubbles make the threshold value of part of the bubble near or same as the threshold value of the background image, the boundary was detected incorrectly and an extra hole might appear inside the bubble as shown in the top left image of the Fig. 4. The frame rate of the SEF-INF2 video was 2800 fps, which means that the duration of one image is less than 0.36 ms, which is small compared to a bubble cycle. If the recognition should repair itself within a figure or two, an effective repair method can be used, even if it itself would make some errors.

The centers of mass (x_0, y_0) were calculated for all recognized bubbles. Also, every pixel of the bubble boundary has its own coordinate pair (x, y). In polar coordinates,

$$x = r \sin\theta \tag{1}$$

and

$$y = r \cos\theta, \tag{2}$$

where r is the distance from the center of mass and θ is the angle. For all recognized objects, the cartesian coordinates have been changed to the polar coordinates and the distances r from the center of mass have been calculated from 0° to 360°. In cases where recognition contains a hole in the bubble and r crosses more than one borderline, a mean value of the coordinates of the lineshave been used for that direction. Fig. 5 presents a border repair method of edge detection.

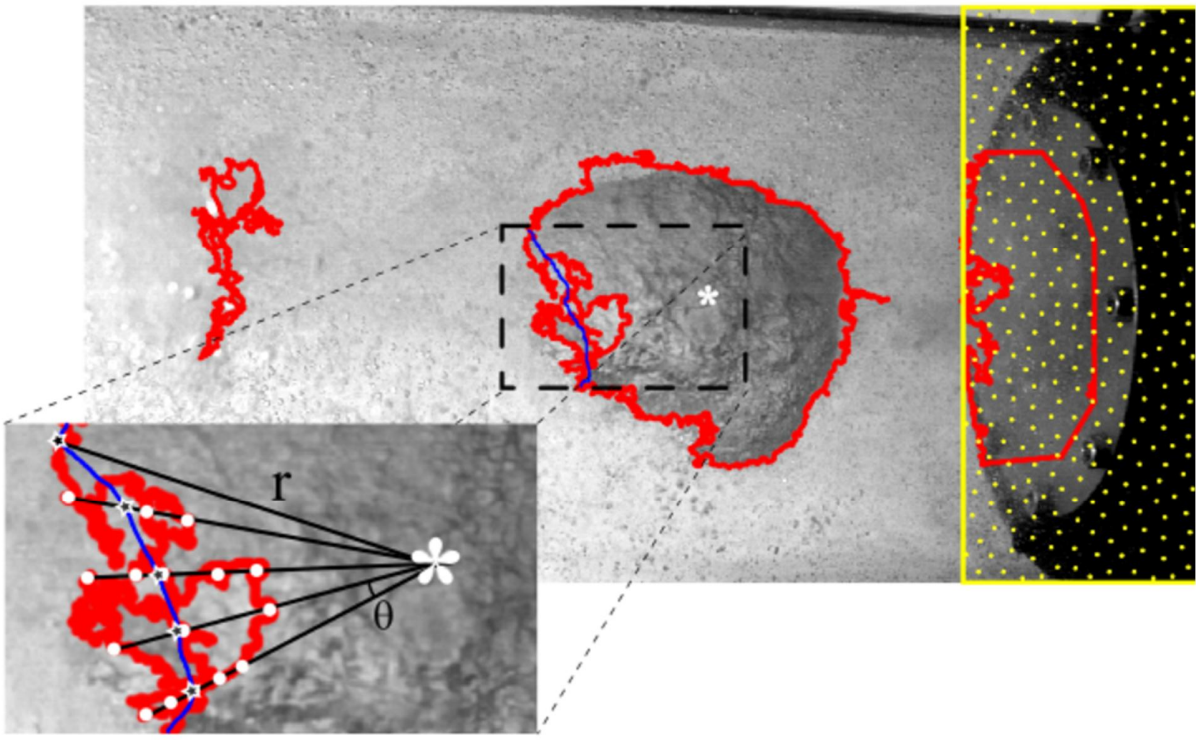

Figure 5. Improving edge detection by the border repair method.

In Fig. 5, the recognized bubble boundary (red) has an issue due to the threshold level of the left border of the bubble. Recognition does not have enough connection points, which makes a hole to the border. The distances r (black lines) from center of mass (white asterisk) in different angles θ are estimated. Due to the incorrect recognition, more than one pixels of the border (white circles) set to the same lines. The distance r was calculated for all border pixels in the same direction and the mean value is calculated (black and white stars). The blue line estimates the corrected bubble border. The method underestimates the border distance but is better than the original recognition. In addition, the maximum value of r could be used instead of mean value, which could overestimate the boundary distance in some cases. It is visible in Fig. 4 and Fig. 5 that at the beginning of the bubble growth near the orifice, pixels of the bubbles have nearly the same threshold value than the threshold value of the orifice plate. Due to this, the orifice plate region, (rectangle with dot pattern in Fig. 5) was cut out from the edge detection. Thus, edge detection takes only into account the detaching bubbles.

When a frame contains more than one bubble, an appropriate tracker algorithm was needed to connect bubbles in subsequent frames to correct bubble tracks. Tracking of the condensing bubbles was based on a Simple Tracker by Tinevez, [14]. The Simple Tracker is a particle tracking algorithm that can deal with 'gaps'. A gap happens when one particle that was detected in one frame is not detected in the next one but appears afterward. If not dealt with, this generates a track break, or a gap, in the frame where the particle disappears, and a false new track in the frame where it re-appears. In this study, the centers of mass of the bubbles act as such particles.

The Simple Tracker needs two input values, the maximum linking distance, and the maximum gap closing. The maximum linking distance defines a maximum value in bubble linking. Two bubbles will not be linked, even if they are the closest pair if the distance of their center of masses is larger than maximum linking distance. The maximum gap closing defines a maximum frame distance in gap closing. Frames further way than this value will not be investigated for gap closing. In this study, 100 pixels (px) (approx. 30 mm) maximum linking distance and the five frames gap closing value was used. In other words, when the bubble grows up tracker tracks the coordinates of the centers of mass. When a growing bubble detaches from the orifice plate and a new bubble starts to grow, this new bubble is linked to the first bubble as long as the distance between the centers of the masses of these two bubbles is smaller than 100 px. 100 px is so near that automatically all of the growing bubbles are marked new bubbles after the first bubble detachment. When a bubble starts to condensate, it might disappear for a while. If the bubble does not reappear within 5 frames, tracking of the bubble ends. If the bubble returns after the five frames gap, it will be marked as a new track, even if the distance between the returning bubble and the previous bubble is less than 100 px.

After all, tracks have been detected, all bubble life cycles should have recorded. The algorithm saves boundary pixel values of all bubbles in every image and calculates corresponding surface velocities and accelerations using the forward difference method. Also, the basic properties of the bubbles, such as volume and surface area could be evaluated.

4. RESULTS AND DISCUSSION

When all of the bubbles were recognized, tracked and linked, the final analysis can be made. Fig. 6 shows the fractions of recognized bubble lifetimes. A total of 67 bubbles were tracked. The mean lifetime of the bubbles was 0.0247 s, and bubble lifetimes varied from 0.0096 s to 0.0361 s. 70 percent of the bubbles had a lifetime between 0.020 s to 0.030 s and approximately 20 percent had the lifetime longer than that, between 0.030 to 0.037 s. All large bubbles of the SEF-INF2 experiment live longer than 20 frames (7.1 ms) and only the tracks longer than this were taken into account. Shorter tracks appeared, for example, when the bubble detached from the orifice plate and the tail of the bubble remained alone for a while. If a new bubble did not appear immediately, the tail was recognized as a useless new short track.

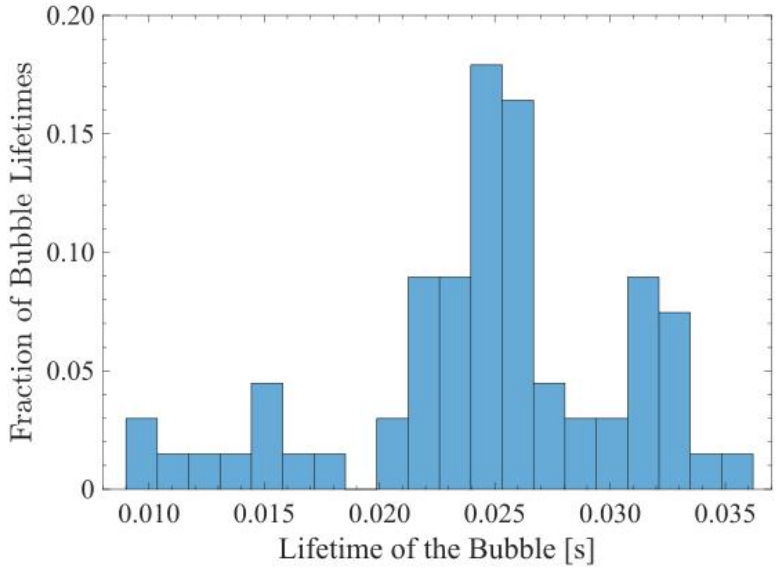

Figure 6. The fraction of 67 tracked bubble lifetimes from the formation to the condensation The maximum linking distance was 100 px, and the maximum gap closing was five frames.

When looking at the formation frequency of the bubbles in Fig. 7 (marked as formation time), it is visible that the formation frequency stayed quite constant during the experiment. Only one longer gap in the bubble formations is visible between 0.52 s to 0.53 s of video sample and one group of increased formation frequency is visible near 0.6 s. The distribution of the formation time between two bubbles is shown in the top of Fig. 8. The line shows a normal distribution fitted to the data. Meantime difference between the bubble formations is 0.0140 seconds ranging from 0.0018 s to 0.0293 s. The line shows normal distribution fitted to data. Mean of normal distribution μ = 0.0139719 s [0.0129682 0.0149755] and standard deviation σ = 0.00408283 s [0.00348571 0.00492874]. The intervals next to the parameter estimates in square brackets are the 95 % confidence intervals for the distribution parameters**.** The corresponding mean frequency of the bubble formation is approximately 71.6 Hz.

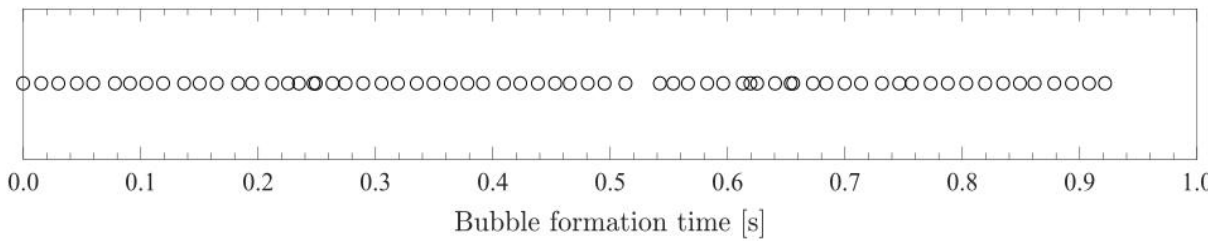

Figure 7. Formation times of the bubbles in the SEF-INF2 experiment.

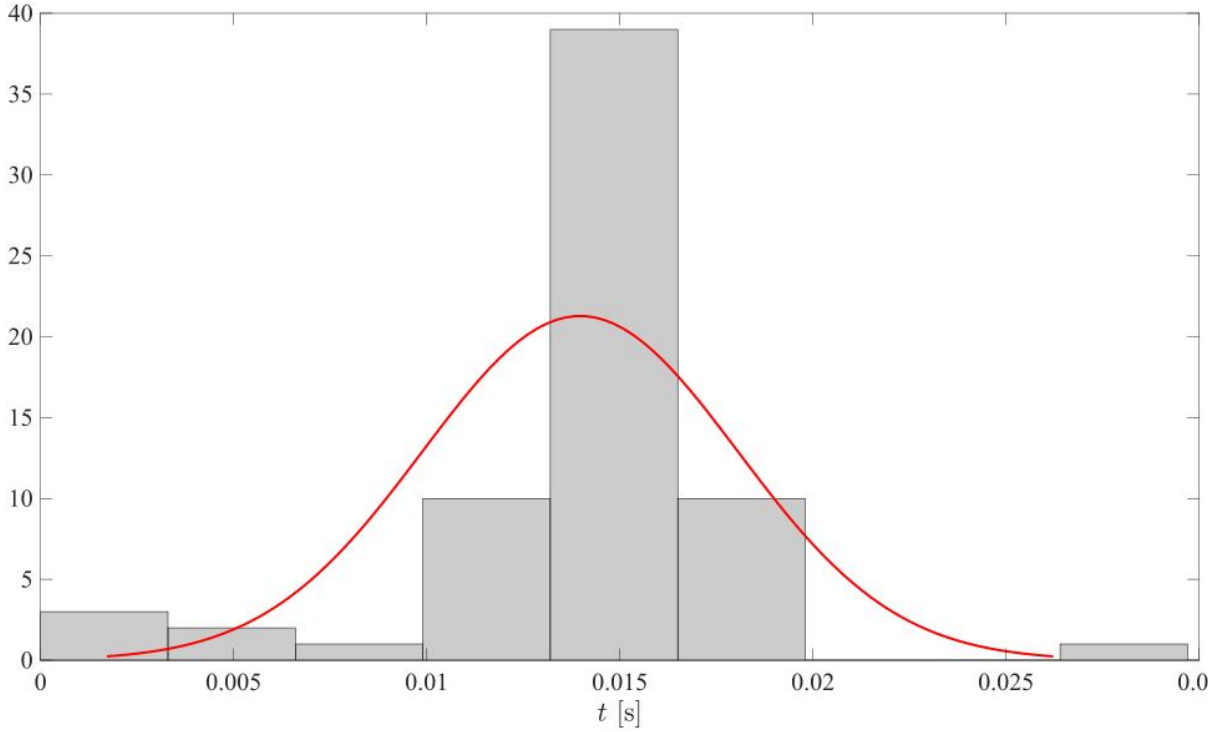

Figure 8. Time difference between two formations of 67 tracked bubbles in the SEF-INF2 experiment.

In the pattern recognition algorithm for the vertical blowdown pipes, [5], only the vertical velocity and acceleration were estimated. In this study, the arbitrary angles between 0° to 360° in 2D plane were estimated (only one camera was available, which provided video of the 2D profile of the bubbles). Fig. 9 and Fig. 10 present velocities and accelerations in different angles θ, for one tracked bubble during its lifetime. The standard polar coordinate system angle directions are used, 0° faces to the orifice and the angle increases counterclockwise.

In the Fig. 9 the positive velocity is to the bubble growing direction, in other words, from right to left. The velocities are plotted in the steps of 45°. The biggest change in the bubble surface velocities can be found in 90° direction – straight upwards. The largest velocities found in this bubble are near 50 m/s. Some bubble surfaces had the velocities larger than 80 m/s. Larger changes can be found also in other upward directions 45°, and 135°. By contrast, the forward direction, 180°, seems to be calm and changes in the velocity small for the whole lifetime of the bubble. Downward directions are quite calm, except 270°, where large, near 30 m/s change occurs at 0.03 s.

Due to the high frame rate, the calculated accelerations of the bubble surfaces grow large. The biggest acceleration difference is near $5 \cdot 10^5$ m/s^2 to upward direction as shown in Fig. 10. To straight upward direction, only one larger change is visible at the middle of the bubbles lifetime. In other upward directions 45° and 135°, larger changes in acceleration can be seen during the whole lifetime of the bubble. Downward directions stay calm, but now horizontal directions 180° and 360° show more activity than the corresponding velocities showed.

Velocities and accelerations for all directions, in a 2D plane between 0° to 360° with 1° interval, were estimated in this study.

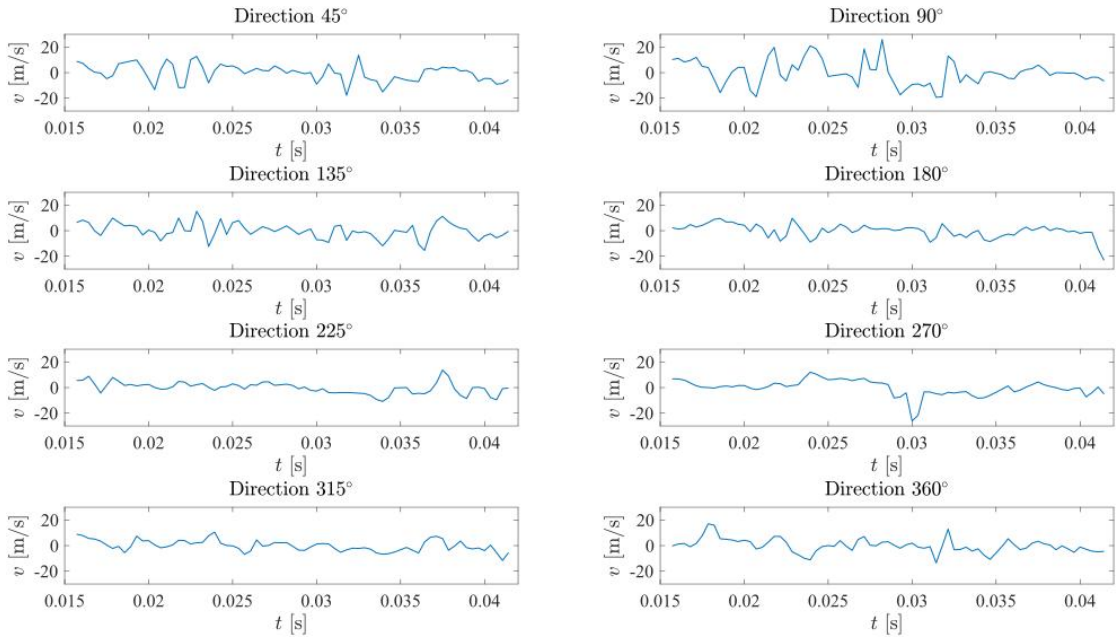

Figure 9. The velocities of one tracked bubble in the different directions from 45° to 360° in the step of 45°.

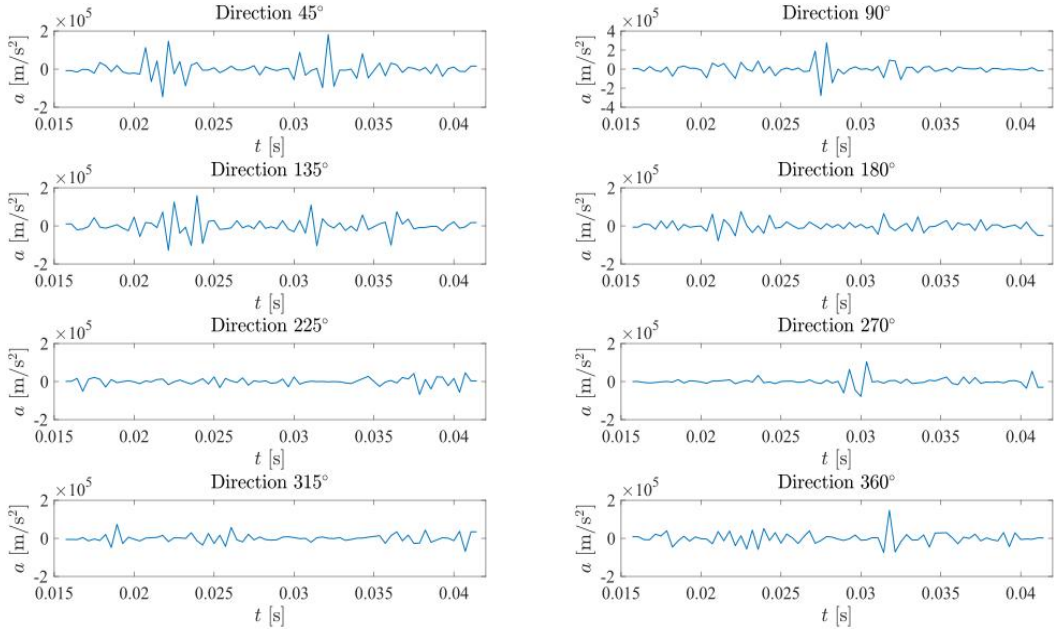

Figure 10. The acceleration of one tracked bubble in the different directions from 45° to 360° in the step of 45°.

5. CONCLUSIONS

The separate effect test facility SEF-POOL was used to study condensation oscillations in a heated up (85 ^{o}C) pool using image analysis. Six, approximately 1-second video shots of the SEF-INF2 experiment were recorded. SEF-INF2-6 test was chosen for this study. The extended pattern recognition based image analysis algorithm was developed and improvements presented in this study. A new algorithm can deal with multiple bubbles, which can temporarily disappear. The algorithm recognizes the bubble boundaries, links bubbles in the subsequent frame to each other, and tracks the whole bubble lifetime.

In total, 67 bubbles were tracked. The mean lifetime of the bubbles was 0.0247 s and the mean time difference between bubble formations was 0.0140 s when corresponding bubble formation frequency was 71.6 Hz. Higher bubble formation frequency shows that the use of a high frame rate is reasonable. In lower frame rates such as 300 fps, two consecutive bubbles might be mixed and misrecognized.

The surface velocities and accelerations were also estimated. The use of only one camera limits the evaluation for a 2D plane which increases errors in cases where bubble path changes from the original axis. Angles between 0^{o} to 360^{o} with a one-degree interval were considered. Velocities were up to 80 m/s and accelerations up to $5 \cdot 10^5$ m/s^2. The highest values were calculated to 90^{o} (straight upward) direction. Forward and backward directions showed calm velocities, but more active accelerations. Downward directions showed mostly calm velocities and accelerations.

Image analysis and pattern recognition have great potential in thermal-hydraulic research. The image analysis algorithm has been improved and works well with multiple bubbles. With suitable video recordings, the algorithm can be used with pipe flows too. Surface velocity and acceleration estimation at arbitrary angles give important knowledge, for example in which direction condensation of the steam bubble begins and will be a good aid for CFD validation purposes.

NOMENCLATURE

BCO	bubbling condensation oscillation
CFD	computational fluid dynamics
CO	condensation oscillation
EHS	effective heat source
EMS	effective momentum source
KTH	Kungliga Tekniska högskolan (Royal Institute of Technology, Stockholm, Sweden)
LOCA	loss-of-coolant accident
LUT	Lappeenranta-Lahti University of Technology LUT
PC	polycarbonate
SEF-INF	test series of the SEF-POOL facility in INFRAL project
SEF-POOL	separate effect facility
SRV	safety/relief valve
VTT	VTT Technical Research Center of Finland LTD

ACKNOWLEDGMENTS

The research leading to these results was partly funded by the Finnish Nuclear Waste Management Fund (VYR) via the Finnish Research Programs on Nuclear Power Plant Safety SAFIR2018 and SAFIR2022. The authors gratefully acknowledge all this support.

REFERENCES

1. R. Lahey and F. Moody, *The Thermal-Hydraulics of a Boiling Water Reactor*, American Nuclear Society, La Grange Park, Illinois, USA, 2. edition, (1993). ISBN: 0-89448-037-5.
2. D. Bestion, "The Difficult Challenge of a Two-Phase CFD Modelling for all Flow Regimes," *Nuclear Engineering and Design,* 279, pp. 116-125, (2014).
3. S. Al Issa, P. Weisensee and R. Macian-Juan, "Experimental Investigation of Steam Bubble Condensation in Vertical Large Diameter Geometry under Atmospheric Pressure and Different Flow Conditions," *International Journal of Heat and Mass Transfer,* 70, pp. 918-929, (2014)
4. V.. Tanskanen, *CFD Modelling of Direct Contact Condensation in Suppression Pools by Applying Condensation Models of Separated Flow*, PhD. Thesis, Lappeenranta University of Technology, (2012).
5. E. Hujala, V. Tanskanen, and J. Hyvärinen, "Pattern recognition algorithm for analysis of chugging direct contact condensation", *Nuclear Engineering and Design*, 332, pp. 202-212, (2018)
6. E. Hujala, *Evaluation of Bubble Formation and Break Up in Suppression Pools by Using Pattern Recognition Methods*, MSc. Thesis, Lappeenranta University of Technology (2013). http://lutpub.lut.fi/handle/10024/89985
7. E. Hujala, V. Tanskanen, and J. Hyvärinen, "Frequency analysis of chugging condensation in pressure suppression pool system with pattern recognition", *Nuclear Engineering and Design*, 339, pp. 244-252, (2018)
8. Gallego-Marcos, I., Filich, L., Villanueva, W., Kudinov, P., "Modelling of the Effects of Steam Injection through Spargers on Pool Thermal Stratification and Mixing", Nordic Nuclear Safety Research, Research Report NKS-347, pp. 1-45. Nuclear Power Safety, Royal Institute of Technology (KTH), Stockholm, Sweden, (2015).
9. Li, H., Villanueva, W., Kudinov, P., "Effective momentum and heat flux models for simulation of stratification and mixing in a large pool of water", Nordic Nuclear Safety Research, Research Report NKS-266, pp. 1-61, Nuclear Power Safety, Royal Institute of Technology (KTH), Stockholm, Sweden, (2012).
10. T. Pättikangas and V. Hovi, "CFD simulation of condensation of vapor jets", VTT Research Report, VTT-R-00993-18, (2018)
11. K. Tielinen, A. Räsänen, E. Kotro, and I. Saure, "General description of SEF-POOL test rig", technical report, INSTAB 2/2017, Lappeenranta University of Technology, (2017).
12. C.H. Song, S. Cho, H.S. Kang, "Steam jet Condensation in a pool from fundamental understanding to engineering scale analysis**,"** *J. Heat Transfer*, **143**, (2012)
13. MATLAB R2016b Academic license, The MathWorks, Inc. (2016)
14. J.-Y., Tinevez, "Simple tracker, version 1.5.0.0", MATLAB Central File Exchange, Retrieved 17 February 2019, https://se.mathworks.com/matlabcentral/fileexchange/34040-simple-tracker